Exploration of metal ion binding sites in RNA folds by Brownian-dynamics simulations

Thomas Hermann and Eric Westhof*

Background: Metal ions participate in the three-dimensional folding of RNA and provide active centers in catalytic RNA molecules. The positions of metal ions are known for a few RNA structures determined by X-ray crystallography. In addition to the crystallographically identified sites, solution studies point to many more metal ion binding sites around structured RNAs. Metal ions are also present in RNA structures determined by nuclear magnetic resonance (NMR) spectroscopy, but the positions of the ions are usually not revealed.

Results: A novel method for predicting metal ion binding sites in RNA folds has been successfully applied to a number of different RNA structures. The method is based on Brownian-dynamics simulations of cations diffusing under the influence of random Brownian motion within the electrostatic field generated by the static three-dimensional fold of an RNA molecule. In test runs, the crystallographic positions of Mg^{2+} ions were reproduced with deviations between 0.3 and 2.7 Å for several RNA molecules for which X-ray structures are available. In addition to the crystallographically identified metal ions, more binding sites for cations were revealed: for example, tRNAs were shown to bind more than ten Mg^{2+} ions in solution. Predictions for metal ion binding sites in four NMR structures of RNA molecules are discussed.

Conclusions: The successful reproduction of experimentally observed metal ion binding sites demonstrates the efficiency of the prediction method. A promising application of the method is the prediction of cation-binding sites in RNA solution structures, determined by NMR.

Address: Institut de Biologie Moléculaire et Cellulaire du CNRS, UPR 9002, 15 rue René Descartes, F-67084 Strasbourg, France.

*Corresponding author.
E-mail: westhof@ibmc.u-strasbg.fr

Key words: hammerhead ribozyme, magnesium ions, RNA aptamers, rRNA, tRNA

Received: **13 May 1998**
Revisions requested: **3 July 1998**
Revisions received: **9 July 1998**
Accepted: **7 August 1998**

Structure 15 October 1998, **6**:1303–1314
http://biomednet.com/elecref/0969212600601303

© Current Biology Ltd ISSN 0969-2126

Introduction

Metal ions play an important role in the folding and stabilization of RNA structure (for reviews see [1,2]). Most classes of catalytic RNA, such as the hammerhead ribozyme and group I introns, require divalent metal ions for catalysis [3]. The binding of metal cations to the polyanionic RNA has been extensively studied, showing that RNA folds can form specific pockets for tight binding of divalent cations [1,2,4]. The positions of metal ions in RNA three-dimensional structures have been revealed in several crystal structures, namely for transfer RNAs (tRNAs) [5–8], the hammerhead ribozyme [9,10], the P4–P6 domain of a group I intron [11], and loop E of 5S ribosomal RNA (rRNA) [12]. Crystal-structure analysis does not, however, exhaustively identify all metal ion binding sites in RNAs, as is indicated by the large number of binding sites observed in measurements carried out on tRNAs in solution [13–15]. More and more three-dimensional RNA structures are derived from nuclear magnetic resonance (NMR) spectroscopy [16,17]. As NMR techniques commonly used for solution-structure determination of RNA do not yield direct information on ion binding, methods were proposed to probe metal binding sites in NMR experiments indirectly [18,19].

Because metal ion binding to RNA results from equilibria between electrostatic and hydration forces, the molding of metal ion binding sites involves more than simply lining the negatively charged phosphate backbone. In the present paper, calculations of the electrostatic field around RNA folds (Figure 1a) were used to find negatively charged pockets suitable for metal ion binding. It is shown that metal ion binding sites of an RNA molecule can be predicted from a given three-dimensional molecular scaffold that defines the arrangement of charges in space. Brownian-dynamics (BD) simulations [20] of cation diffusion were used to identify possible metal ion binding sites in RNA. Trajectories of positively charged test spheres moving under the influence of both random Brownian motion and the electrostatic field of the target RNA molecule were simulated (Figure 1b). Electrostatic interactions were calculated with the non-linear Poisson–Boltzmann equation [21] and a continuum model for the solvent. Potential metal ion binding sites were identified as regions of the RNA in which a significant number of the randomly diffusing test charges are finally trapped following interaction with the RNA electrostatic field. In contrast to simpler methods that merely rely on visual inspection of the electrostatic field, the BD simulations of

Figure 1

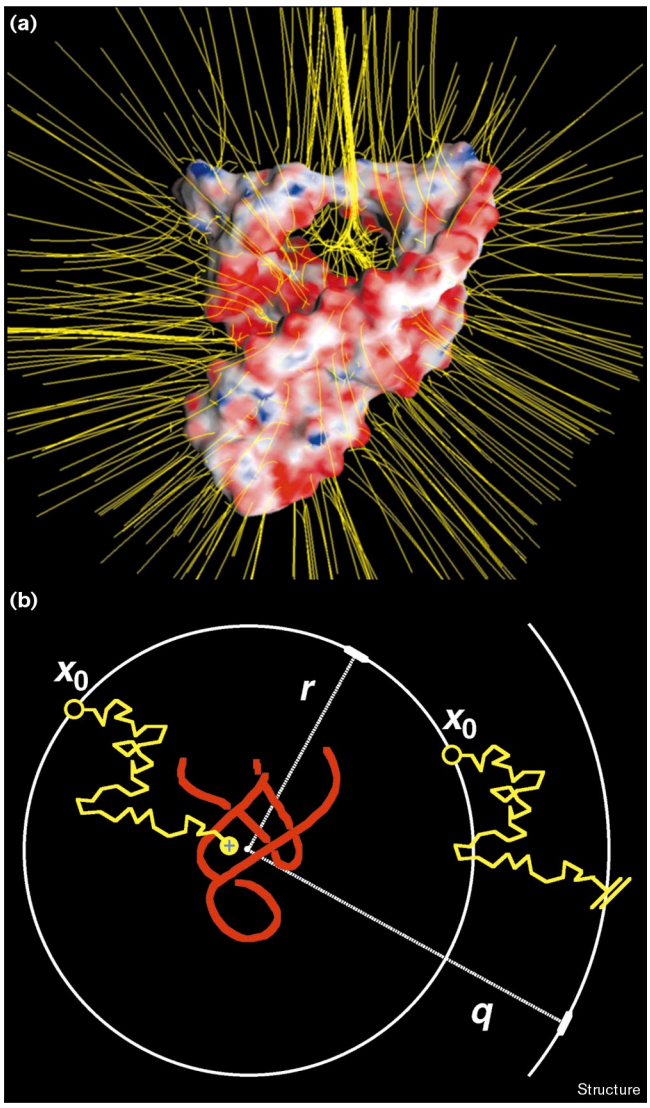

Exploration of the electrostatic field around RNA by simulation techniques. **(a)** The electrostatic field around the three-dimensional fold of an RNA molecule is formed by the spatial arrangement of charged atoms. Amongst these the negative phosphates dominate, thereby creating strong attractors for positive charges as illustrated by the bundles of field lines (yellow) emerging from the central cavity of the hammerhead ribozyme RNA. Negative surface charge is colored red, positive charge blue. **(b)** In BD simulations of metal ion binding to RNA, diffusible metal ions are simulated by charged test spheres moving under the influence of both random Brownian motion and the electrostatic field generated by the RNA. Simulations are initiated by placing the probe at randomly chosen points x_0 at a distance r from the RNA center of mass. Trajectories are calculated over a large number of steps, except for probes exceeding the outer cutoff distance q. Potential Mg^{2+}-binding sites are those regions of the RNA where the randomly diffusing test charges are finally trapped by interacting with the RNA.

diffusing test spheres yield an objective and more complete picture of both the gradient of the electrostatic field and its minima, which correspond to electronegative pockets suitable for metal ion binding. Beyond electrostatic interactions, geometrical factors, such as the space available for a hydrated metal ion, are considered during the selection of binding sites. As a result of the spherical shape of the diffusing probes, subtle differences in the coordination geometry of negatively charged pockets are out of reach of the present BD simulation method. However, the size of the cations was taken into account by running several sets of BD simulations in which the radii of the diffusing test spheres were varied.

Here, we describe the results of BD simulations performed on the crystal structures of loop E of 5S rRNA, $tRNA^{Phe}$, $tRNA^{Asp}$, and the hammerhead ribozyme. Negatively charged pockets corresponding to metal ion binding sites are successfully calculated for most of the metal cations found in the crystal structures. Additional metal binding sites in RNA folds are predicted, for example for the tRNAs, in line with experimental findings from solution studies. Further, predictions of metal ion binding sites are made for five different RNA structures previously determined by NMR spectroscopy.

Results and discussion

Loop E of bacterial 5S rRNA

Bacterial 5S rRNA is part of the 50S ribosomal subunit and contains the internal loop E domain, a region of non-Watson–Crick base pairs that becomes structured only in the presence of Mg^{2+} ions [22]. Five RNA-bound Mg^{2+} ions have been identified in the crystal structure of a duplex dodecamer encompassing loop E of *Escherichia coli* 5S rRNA [12]. Three of the Mg^{2+} ions (B, C, and E) are directly coordinated to the RNA, but two others (A and D) are bound via water molecules (Figure 2a). After removal of the Mg^{2+} ions, the loop E duplex dodecamer was used as a target in a series of BD simulations with cationic probes of radii varying in steps of 0.1 Å between 1.0 and 1.8 Å, and in steps of 0.5 Å between 2.0 and 3.0 Å. For radii below 1.8 Å, a large number of diffusing probes were trapped in the proximity of the Mg^{2+} sites B, C, and D, resulting in a good match between the calculated density and the crystallographic metal binding sites (Figure 2a). Probes with radii greater than 1.8 Å were mostly trapped outside the deep groove and in the proximity of the Mg^{2+} sites A and E. Three Mg^{2+} ions could be placed in the three-dimensional structure of loop E RNA, at the highest occupations in the density map resulting from the 1.2 Å probe (corresponding to the crystallographic B, C, and D sites). Deviations between calculated and crystallographical Mg^{2+} positions were between 1.3 and 1.8 Å (Figure 2a).

In a second series of BD simulations, loop E RNA, along with the three Mg^{2+} ions at the calculated positions (equivalent to the B, C, and D sites), was used as a target for diffusing probes of radii between 2.0 and 3.0 Å. For the

Figure 2

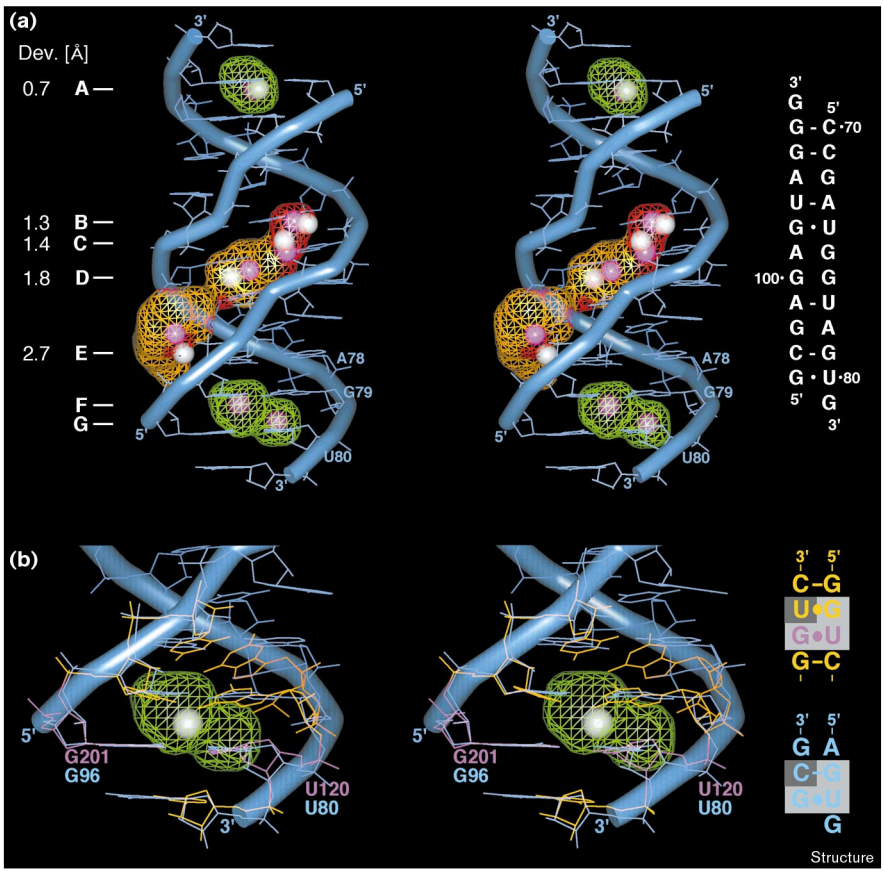

Stereoview of a comparison between Mg^{2+}-binding sites determined by X-ray crystallography [12] and by BD simulations on the crystal structure of a duplex dodecamer encompassing the internal loop E of *E. coli* 5S rRNA. **(a)** Crystallographic Mg^{2+} ions are shown as white spheres. Volume elements of high residence time for +2*e*-charged test spheres in BD simulations are visualized as a density grid, which is in orange for probes with 1.2 Å radius and in green for 2.2 Å probes. Sites of highest occupation are in red. Purple spheres depict the positions of Mg^{2+} ions calculated from the theoretical density. The deviation between crystallographic and calculated positions is given on the left. Mg^{2+} sites F and G are predicted from BD simulations and are not observed in the crystal structure. On the right, a secondary structure representation reflecting the pairing and stacking pattern observed in the crystal structure is shown. **(b)** Comparison between the metal ion binding sites F and G and a tandem of G·U pairs in the J4/5 junction of a group I intron where a metal ion (white sphere) is bound in the crystal structure [4]. 5S rRNA is in blue; intron RNA is in orange, apart from the intron G·U pair used for superimposing the structures, which is in magenta. The insert on the right compares the 5′-GU-3′/3′-CG-5′ motif in loop E RNA (bottom), which is a predicted metal ion binding site, with the corresponding 5′-GU-3′/3′-UG-5′ motif from the group I intron (top).

2.2–2.3 Å probes, the density of trapped cations coincided best with the crystallographic Mg^{2+} A and E sites (Figure 2a). Two Mg^{2+} ions placed according to the calculated density peaks of the 2.2 Å probe deviated from the crystallographic positions by 0.7 and 2.7 Å for sites A and E, respectively. In addition to sites A and E, two overlapping density peaks were found that did not match any of the crystallographically identified metals. Mg^{2+} at these predicted sites (F and G; Figure 2a) may form contacts to $A_{78}(OP_{R,S})$, $U_{80}(O4)$ (both sites F and G) and to O6 (F) and OP_R (G) of G_{79}. The distance between ions placed at sites F and G is only 4.0 Å, and the overlap between the corresponding density peaks may point to a delocalized site where a single metal ion binds in a disordered fashion. The delocalized character, along with the lack of potential coordinating atoms in a suitable geometry, may prevent Mg^{2+} ions from binding with high occupancy to this site, which could therefore probably be filled either by a monovalent cation less dependent on octahedral coordination or by an electrostatically restricted water molecule.

The predicted F and G sites, located in the deep groove at the level of the G_{96}·U_{80} pair, share remarkable structural similarity with the metal ion binding sites at G·U pairs in the J4/5 junction of group I intron (Figure 2b). Cate and Doudna [4] have proposed that G·U pairs may play a structural role in forming specific binding sites for metal ions. Results from our BD simulations are in agreement with this view, suggesting that 5′-GU-3′/3′-YG-5′ motifs (where Y is a pyrimidine residue) form metal ion binding sites in the deep groove of double-stranded RNA helices. Interestingly, the metal ion binding site in P5 of group I intron, which comprises the 5′-GU-3′/3′-YG-5′ motif, appears to bind preferentially to hexammines and not to hexahydrated Mg^{2+} ions [4]. This might account for the fact that a Mg^{2+} ion is not seen at the F or G sites in the crystal structure of loop E RNA, despite the fact that the BD simulations predict a negatively charged pocket there. Cate and Doudna [4] have suggested that subtle details in the coordination geometry of a site may account for the discrimination between hexammines and hexahydrates. Hexammines are, like monovalent cations, less dependent on an octahedral coordination and may thus overcome a more distorted binding geometry at 5′-GU-3′/3′-YG-5′ tandems because of additional hydrogen-bond donors on the ion [23].

The positioning of Mg^{2+} ions within the density peaks obtained by BD simulations was straightforward for the roughly spherically shaped peaks that were used to place single cations at the center of mass. However, for density peaks of elongated or complex shape, the choice of the number of ions that ought to be placed was less obvious. For elongated peaks we used an automated search procedure in order to find the optimum fit for two Mg^{2+} ions.

The approach of running two different surveys using smaller (1–2 Å) and larger (2–3 Å) probes was devised to account for differences between sites where the Mg^{2+} ion is directly coordinated to RNA from sites where the Mg^{2+} ion binds via its hydration shell. Sterical effects, beyond purely electrostatical interactions, can thus be taken into account. An increased accuracy in the prediction of the binding sites for hydrated Mg^{2+} ions in the loop E dodecamer was achieved by running BD simulations on the RNA with the Mg^{2+} ions initially placed at positions found with the smaller probes. The presence of the directly coordinated Mg^{2+} ions provided a filter for screening the negatively charged pockets not sterically accessible to the larger hydrated Mg^{2+} ions.

tRNAs

The tRNAs were the first RNAs for which three-dimensional structures were available [24]. The complex three-dimensional fold of tRNA contains numerous metal ion binding pockets. Solution studies have shown that 3 to 4 strong ($K_d \approx \mu M$) and more than 20 weak Mg^{2+}-binding sites exist in tRNAs [1,2]. Crystal-structure analysis of the orthorhombic form of yeast $tRNA^{Phe}$ [24] revealed four Mg^{2+} ions bound in loop regions [5]. BD simulations with test spheres of 1.0–3.0 Å radius were carried out on the refined X-ray structure of both naked $tRNA^{Phe}$ [25] and $tRNA^{Asp}$ [26]. Analysis of the density peaks at locations where the majority of diffusing probes were trapped by electrostatic interaction with the tRNAs revealed at least 14 potential metal ion binding sites in $tRNA^{Phe}$ (Figure 3a). The four crystallographic Mg^{2+} sites in $tRNA^{Phe}$ are located within density peaks calculated from the BD simulations. Site 1 is situated in the P10 loop. Two Mg^{2+} ions are found in the D loop (sites 2 and 3) where, close to site 3, a Pb^{2+} ion can substitute for a Mg^{2+} ion [27]. Among the calculated sites, a sharp density peak in the anticodon loop of $tRNA^{Phe}$ coincided exactly with the crystallographic Mg^{2+} at site 4, which deviates less than 0.4 Å from the peak center of mass. Deviations between calculated and crystallographic Mg^{2+} positions for sites 1, 2, and 3 were between 2.1 and 2.6 Å for $tRNA^{Phe}$ (Figure 3a).

The crystal structure of $tRNA^{Asp}$ contains a single Mg^{2+} located in the anticodon loop at the deep groove face of the $C_{31}.G_{39}$ base pair [26]. This position was not found with any of the test spheres used in BD simulations. With the 2 Å probe, however, a strong density peak indicative of a metal ion binding site was found at a distance of 5 Å, shifted upward in the anticodon stem at the $G_{30}{\cdot}U_{40}$ wobble pair (Figure 3b). The density is located in a 5′-GU-3′/3′-YG-5′ structural motif equivalent to the metal ion binding sites predicted in proximity of a G·U pair in loop E RNA (see above) and experimentally found at G·U pairs in the crystal structure of P4–P6 of group I intron (Figure 2b). The deviation between the crystallographically determined Mg^{2+} ion and the calculated electronegative pocket may indicate a delocalized binding of metal ions in the anticodon loop of $tRNA^{Asp}$, in contrast to $tRNA^{Phe}$ where the crystallographically determined Mg^{2+} is found with high precision by BD simulations (see above). As was discussed above for the loop E RNA, delocalized metal ion binding in the anticodon loop of $tRNA^{Asp}$ could be linked to a distorted coordination geometry at the 5′-GU-3′/3′-YG-5′ tandem. Interestingly, the anticodon loop of $tRNA^{Phe}$ does not contain the 5′-GU-3′/3′-YG-5′ motif. Metal ion binding sites corresponding to the positions of Mg^{2+} sites 1–3 in the crystal structure of $tRNA^{Phe}$ were predicted for $tRNA^{Asp}$, too (data not shown). For both tRNAs, BD simulations predicted at least 10 preferred sites for metal ion binding that do not overlap with the crystallographically determined ion positions. Seven of the additional sites have an almost spherical shape and are located close to phosphates of the RNA backbone, namely in the acceptor stem (four sites), in the T loop (one site) and in the anticodon loop (two sites). Two of the predicted sites located at the 5′ and 3′ termini in the acceptor stem are not relevant because the pronounced dynamics of the ends of the tRNA are not taken into consideration. Interestingly, a binding site is predicted in the vicinity of pseudouridines in the anticodon loop of both tRNAs (Ψ_{39} in $tRNA^{Phe}$, Ψ_{32} in $tRNA^{Asp}$). This site corresponds to the position of long-lived water molecules at pseudouridines observed in both crystal structure analysis [24] and molecular-dynamics simulations of $tRNA^{Asp}$ [28]. It is expected that some of the binding sites predicted on the basis of their electrostatic environment are occupied by long-lived and electrostatically restricted water molecules.

We found no structural characteristics that were able to discriminate between calculated sites that coincide with crystallographic metal ions and calculated sites that lack counterparts in the X-ray structure. Because of both this ambiguity and the fact that all crystallographic Mg^{2+} ions had been covered by density peaks from the first set of simulations, the approach of running two different BD surveys (see above) was not used for the tRNAs. The most extensive region calculated as a binding site for positively charged probes in both tRNAs is located in the deep groove near the junction of the anticodon stem and D stem where, in the crystal structure of $tRNA^{Phe}$, a molecule of polycationic spermine binds (Figure 3a) [7]. Spermine is used for growing well-ordered crystals of tRNA

Figure 3

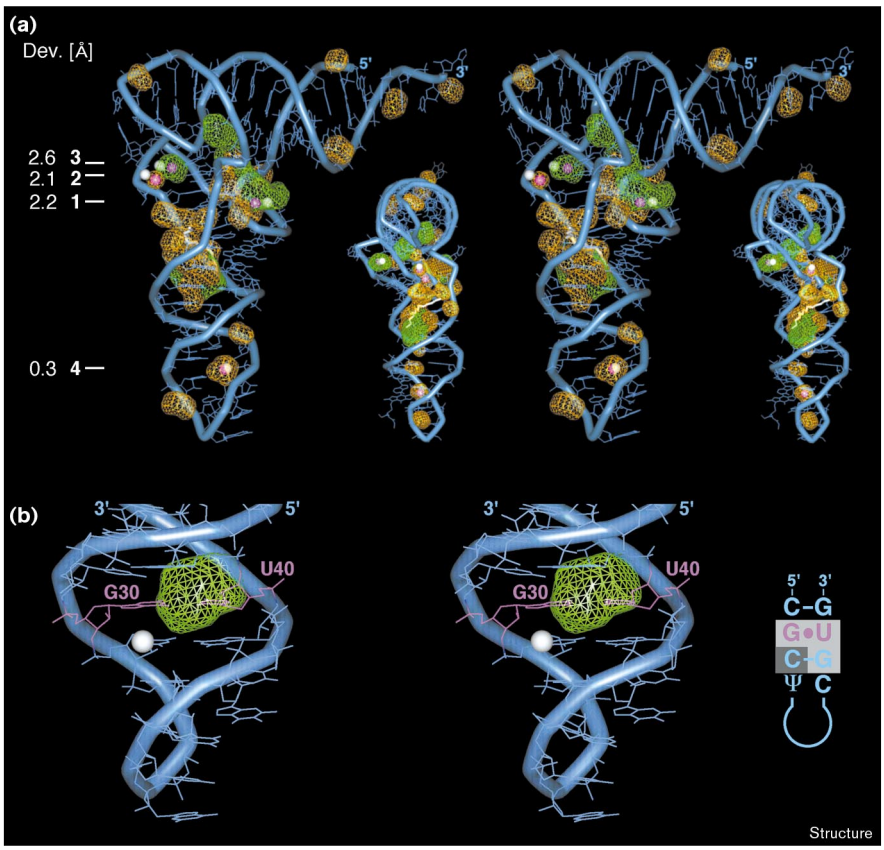

Stereoview of metal ion binding sites predicted by BD simulations on the X-ray structure of $tRNA^{Phe}$ [25]. **(a)** Calculated densities, and crystallographic and predicted Mg^{2+} sites are represented as in Figure 2. Crystallographic Mg^{2+} sites are numbered according to Holbrook *et al.* [5]. A spermine molecule in the major groove of the acceptor stem is shown in stick representation (white). The insert shows the tRNA rotated by 90°, looking from the T loop along the acceptor stem. The deviation between crystallographic and calculated positions is given in the left margin. **(b)** The anticodon loop of $tRNA^{Asp}$ with a bound Mg^{2+} ion (white sphere) as seen in the crystal structure [26]. The BD simulations predict a metal ion binding site shifted by 5 Å in comparison to the crystallographic Mg^{2+}. The calculated site is located at the major groove face of the $G_{30}{\cdot}U_{40}$ base pair. The G·U wobble pair in the $tRNA^{Asp}$ anticodon loop is part of a 5′-GU-3′/3′-CG-5′ motif that is proposed to be a metal ion binding site also present in loop E of *E. coli* 5S rRNA and group I intron (see Figure 2b).

suitable for X-ray diffraction [29,30] and it is likely that in the absence of spermine, polyamine-binding sites are occupied by metal cations. At such sites, Zn^{2+} and Sm^{3+} are found in crystals of $tRNA^{Phe}$ soaked with the metal ions [6,31]. The extended shape of the density peak that coincides with the spermine-binding site suggests that metal ions may bind in a delocalized fashion in the deep groove. Around Mg^{2+} site 1, a similar delocalized density that overlaps with a large peak inside the hinge between loops T and D is found.

Hammerhead ribozyme RNA

The hammerhead ribozyme is a small RNA motif that catalyzes the cleavage of a phosphodiester bond within its own backbone (for review see Birikh *et al.* [32]). Catalytic activity of the hammerhead ribozyme depends on the presence of metal ions that are required for both folding [33,34] and cleavage catalysis [32]. Divalent metal ions contribute to the chemical step of phosphodiester-bond cleavage [35] by providing a metal-bound hydroxo group that activates the cleavage-site 2′-OH for attack at the adjacent phosphorous [36,37]. Crystal structure analyses of hammerhead ribozymes have revealed the positions of five Mg^{2+} ions and a Mn^{2+} ion bound to the RNA [9,10,38].

We performed BD simulations, with test spheres of 1.0–3.0 Å radius, on the crystal structure of a freeze-trapped catalytic hammerhead intermediate [38] after removal of the crystallographic metal ions (Figure 1a). A large number of the diffusing probes were trapped in the cavity formed by the facing deep grooves of stems I and II in the hammerhead RNA fold (Figure 4). The density peaks obtained with probes of different radii extended throughout the whole cavity, continuing into the deep groove of stem III. In contrast to the distinct and separate metal ion binding sites predicted for the crystal structures of loop E RNA and the tRNAs (see above), the preferred positions for cation binding are strongly overlapping in the hammerhead RNA, leading to merging and continuous density. Of the six metal ions (designated sites 1–6) identified in the crystal structure of the freeze-trapped catalytic hammerhead intermediate, five were located within density peaks calculated from BD simulations (Figure 4). Two metal ions, namely Mg^{2+} at site 6, which is directly bound to the pro-R_P oxygen of the cleavable phosphate, and Mn^{2+} at site 5 are both located within protrusions of the 1 Å density grid, whereas the three metal ions at sites 1, 2, and 3 lie in the less structured regions of the calculated density.

Figure 4

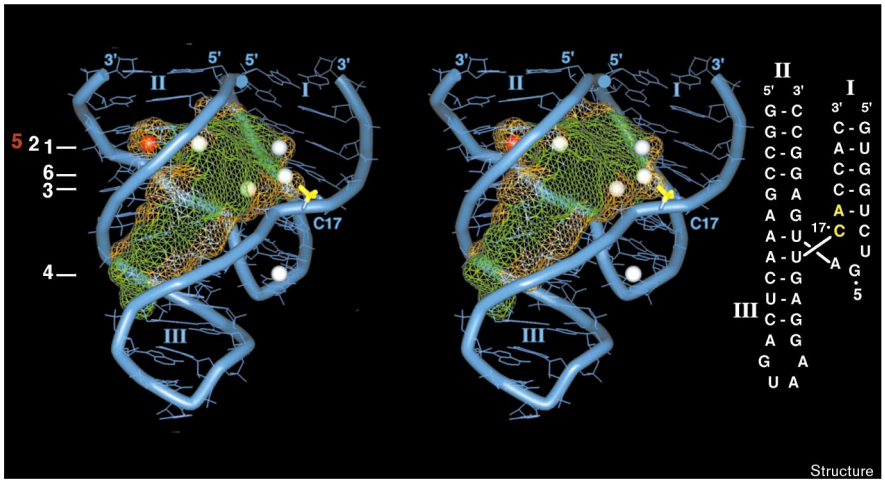

Stereoview of the three-dimensional structure of hammerhead ribozyme RNA determined by X-ray crystallography [38]. The three stems are designated I, II and III. The phosphate at the cleavage site between C_{17} and $A_{1.1}$ is marked in yellow. Mg^{2+} ions present in the crystal structure of a freeze-trapped catalytic hammerhead intermediate are depicted as white spheres numbered 1–4 and 6, according to the convention adopted in [38]. Site 5 binds Mn^{2+} (red sphere), but not Mg^{2+}, whereas sites 1, 3 and 4 bind both metals at similar positions (only Mg^{2+} shown). Densities of trapped positively charged probes from BD simulations are represented as in Figure 2. The secondary structure representation (right) reflects the pairing and stacking pattern observed in the crystal structure along with the nucleotide-numbering scheme of Scott *et al.* [38].

No density was found for metal site 4 at G_5 of the hammerhead RNA and analysis of the calculated trajectories revealed that none of the diffusing probes was trapped around that position. Although a Mg^{2+} ion is found at site 4 in the crystal structure, inspection of the electrostatic potential, in agreement with previous observations [39], did not reveal a negatively charged surface patch in this region. On the basis of pure electrostatics, site 4 appears to be an unfavourable place for a metal cation. It is therefore possible that a crystal lattice contact is responsible for Mg^{2+} binding at site 4. Another explanation could be that metal ion binding at site 4 depends entirely on coordination contacts in order to overcome the unfavourable charge distribution that surrounds this site. Fluorescence measurements [34] and experimental data on the inhibition of hammerhead catalysis by terbium(III) [40] indicate that a metal ion bound to G_5 may be required during the folding process but that it is released before the transition state is achieved [40]. It has been demonstrated that the Mg^{2+} ion bound to G_5 is not essential for the transition-state structure [40]. Another Mg^{2+}-binding site in the junction between the stacked stems II and III at the phosphates of A_{13}/A_{14}, which was proposed by Chartrand *et al.* [39], is also covered by the 1 Å density grid.

The relatively extended and undifferentiated density of the peaks calculated from BD simulations in the hammerhead ribozyme contrasts with the well-defined peaks calculated for the E loop and tRNAs. This observation may reflect an intrinsic property of the wishbone-like RNA fold acting as a primitive electrostatic trap for divalent metal ions (Figure 1a). In support of this hypothesis are the low occupancy of the Mg^{2+} ions in the crystal structure, the broad distribution of Mg^{2+}-binding processes observed in fluorescence measurements of the hammerhead ribozyme [41], and the low binding constants for divalent metal ions, which are approximately 100-fold weaker than the binding constants for site-specific cation binding to tRNA [41,42]. Thus, after folding of the hammerhead RNA, a process that requires the binding of up to two Mg^{2+} ions [34], a large electronegative cavity that attracts cations in a rather unspecific fashion, but with increased affinity, is created. In turn, the gathered metal ions stabilize the hammerhead fold [33]. As a result of Mg^{2+} ions becoming trapped in the hammerhead cavity at an increased concentration relative to the ions in bulk solution, ions may more frequently occupy positions close to the cleavage site and catalyze the phosphodiester bond cleavage that occurs after an occasional C3′-*endo* to C2′-*endo* conformational flip in the C_{17} ribose [37,43] as was recently proven by X-ray crystallography [44]. It is tempting to speculate that the noncooperative dissociation of divalent metal ions that accompanies hammerhead-ribozyme catalysis [42] could be the release of cations as a result of disruption of the electronegative cavity between stems I and II, due to increased flexibility of the RNA after backbone cleavage.

The supposition that the hammerhead fold acts as a rather unspecific electrostatic trap for positively charged species is supported by our recent work on the mechanism of cleavage inhibition of the hammerhead ribozyme by aminoglycoside antibiotics such as neomycin [45]. It was suggested that binding of the polycationic aminoglycosides displaces the Mg^{2+} ions required for catalysis from the electronegative cavity of the hammerhead ribozyme. Several different conformations of the flexible aminoglycosides could be docked to the hammerhead cavity, such that the positively charged ammonium groups of the drugs pointed towards regions of highest electronegativity [44].

Figure 5

Stereoview of the NMR structure of the P5b stem loop of a group I intron complexed with cobalt(III) hexammine [18]. The metal complex is represented by spheres (Co(III), magenta; NH_2 ligands, blue). The density grid (orange) was obtained from BD simulations of test spheres with a radius of 1.5 Å. A representation of the secondary structure of the RNA is shown on the right.

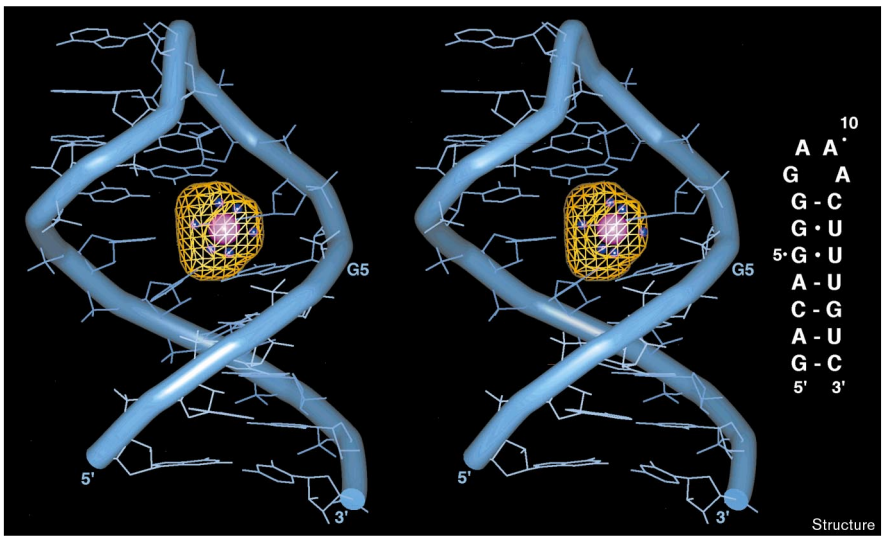

RNA structures from NMR spectroscopy

The ordered three-dimensional folding of RNA is dependent on the presence of metal ions that are not detectable in most NMR experiments. Methods for probing metal binding sites in RNA indirectly by NMR experiments were proposed only recently [18,19]. As we obtained encouraging results in using the BD method on the prediction of metal ion binding sites for crystal structures of RNAs, we have used the method to explore possible metal ion binding sites in NMR structures. We will discuss the results obtained on the P5b stem loop from group I intron [18], an RNA pseudoknot [46], and the sarcin/ricin loop RNA [47]. Further predictions of metal ion binding sites will be presented for aptamers of flavin mononucleotide (FMN) [48] and adenosine monophosphate (AMP) [49], which are molecules obtained by artificial *in vitro* selection that bind small ligands with high affinity [50].

Kieft and Tinoco have used NMR spectroscopy to determine the binding position of a cobalt(III) hexammine ion in the three-dimensional structure of an 18-base oligonucleotide corresponding to the P5b stem loop of group I intron ribozymes [18]. They suggested that the ability of cobalt(III) hexammine to induce chemical-shift changes and to display intermolecular nuclear Overhauser effects (NOEs) to the RNA renders it a general probe of metal ion–RNA interactions [18]. BD simulations on the P5b stem-loop RNA in the absence of the cobalt(III) hexammine complex reproduced with high precision the experimentally observed binding site of the metal ion (Figure 5). The center of mass of the density calculated from BD simulations with a 1.5 Å test sphere deviates less than 0.9 Å from the Co(III) position in the NMR structure. Rewardingly, only a single metal ion binding site was predicted by the simulations, consistent with the experimental findings. The excellent agreement between the experimentally determined and the predicted binding site for the Co(III) ion in the P5b stem-loop RNA suggests that the BD-based prediction method can be faithfully applied to RNA structures determined by either NMR or X-ray crystallography.

RNA pseudoknots are particularly interesting test cases for the BD prediction method, as either divalent metal ions or a high concentration of monovalent cations is necessary for pseudoknot formation [51]. We used BD simulations of cation diffusion to explore possible metal ion binding sites in the pseudoknot formed by the 34-nucleotide RNA called VPK, the three-dimensional structure of which has been determined by NMR spectroscopy [46]. The calculations suggest that three negatively charged pockets that are suitable for metal ion binding exist within the VPK RNA (Figure 6 and Table 1). Site 1 comprises nucleotides of both the interhelical junction and loop L2. It has been suggested that metal ions might be required to stabilize the helix junction in RNA pseudoknots [52]. Sites 2 and 3 are formed by nucleotides of stem S2 and loop L1. At these sites, binding of cations is probably necessary to shield the electrostatic repulsion of the compactly folded backbone in the L1 loop.

The three-dimensional solution structure of a 29-base oligonucleotide comprising the α-sarcin/ricin-sensitive loop from rat 28S rRNA has been determined by NMR spectroscopy [53]. The sarcin/ricin loop structure reveals a highly ordered conformation maintained by base pairing and stacking in three segments that are common motifs of RNA structure, namely a GNRA-type tetraloop (where R is a purine and N is any residue) [54], a bulged-G motif,

Figure 6

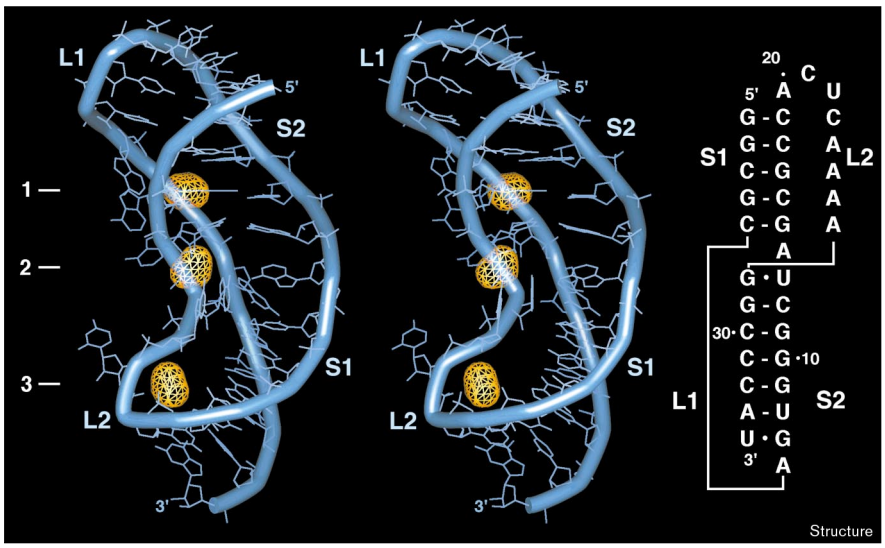

Stereoview of the three-dimensional structure of an RNA pseudoknot determined by NMR spectroscopy [46]. Three predicted metal ion binding sites (1–3) are shown as density grids, as in Figure 2. The secondary structure of the RNA, along with the designation of the stems and loops, is depicted on the right.

and an A-type stem. For the sarcin/ricin loop, BD simulations reveal seven independent sites on the RNA as possible candidates for binding metal ions (Figure 7 and Table 1). Four sites (1, 3, 4, and 5) are located at or in the proximity of the bulged-G motif. Two further sites (6 and 7) are found in the A-type stem and one site (2) is provided by the GNRA tetraloop. The upper region of the sarcin/ricin loop comprises five possible cation-binding sites and, thus, is especially implicated in the specific interaction of 28s rRNA with basic side chains of proteins such as ricin and α sarcin, known to recognize the top region of the RNA loop [53,55].

Table 1

Predicted binding sites for metal ions in NMR structures of RNA molecules.

Site	Involved nucleotides	Motif	X, Y, Z*
VPK pseudoknot†			
1	G_4(O2′, base), C_5(O4′), A_{25}(O3′, O4′), A_{26}(O5′)	Stem loop	10.0, 11.3, −1.6
2	A_6(OP, base), G_7(base)	Loop	6.2, 3.1, −6.6
3	G_7(O3′), G_9(OP, base), G_{10}(OP, base)	Stem loop	3.5, 1.5, −18.3
α-Sarcin/ricin-sensitive loop‡			
1	G_{10}(O2′), U_{11}(OP), G_{18}/G_{19}(base)	Bulged G	4.9, 9.7, 4.3
2	A_{12}(OP), C_{13}/G_{14}(base)	GNRA loop	−0.1, 8.1, 8.2
3	A_9(base), A_{20}/A_{21}(OP)	Bulged G	−5.0, −2.4, −0.8
4	A_9(OP, base), C_8/C_{22}(O2′), A_{21}(base)	Bulged G	5.2, −1.1, 4.4
5	C_8/G_{10}(OP), A_9(O2′)	Bulged G	−0.3, −5.1, 11.1
6	G_{24}(OP, base),	Stem	5.2, −12.0, 2.3
7	G_2-G_5(OP, base)	Stem	−, −, − (delocalized)
FMN aptamer§			
1	A_{11}(O2′, base), U_{14}–C_{16}(base)	Stem	−13.6, −17.8/0.3
2	G_{10}/G_{24}(base), A_{23}(OP)	Ligand pocket	−11.0, −10.0, −5.7
3	G_9/G_{27}/G_{28}(base), A_{26}(OP)	Ligand pocket	−11.7, 0.0, 4.2
4	G_1(O5′), G_2/G_{27}/G_{28}(OP)	Stem	−13.4, 2.9, 8.9
5	G_1(O5′), G_2(OP), G_4/U_5(OP, base)	Stem	−11.5, 8.3, 6.6
6	C_{30}/A_{31}(OP), C_{35}(O2′)	Stem	3.0, 7.9, 6.1
AMP aptamer¶			
1	A_{12}/G_{34}(OP), C_{35}(base)		0.9, 4.8, 3.1
2	G_6–G_8(base), G_{11}(OP)		−2.8, 1.2, 7.2
3	A_{12}(O2′), A_{14}/A_{33}(OP), G_{34}(base)		−9.4, −3.3, 6.7
4	A_{10}(O2′), G_{11}(OP), A_{14}/C_{15}(base)		−5.9, −1.9, −1.5

*Atomic coordinates X,Y,Z refer to the orthogonal coordinate systems of the original PDB files (see Materials and methods section). †[45], Figure 6; ‡[53], Figure 7; §[56], Figure 8; ¶[57], Figure 9.

Figure 7

Stereoview of the three-dimensional solution structure of the α-sarcin/ricin-sensitive loop from eucaryal 28S rRNA, as determined by NMR spectroscopy [53]. Possible metal ion binding sites (1–7) predicted by BD are depicted by density grids, as in Figure 2. The secondary structure based on the pairing and stacking of nucleotides observed in the NMR structure of the sarcin/ricin loop is given on the right.

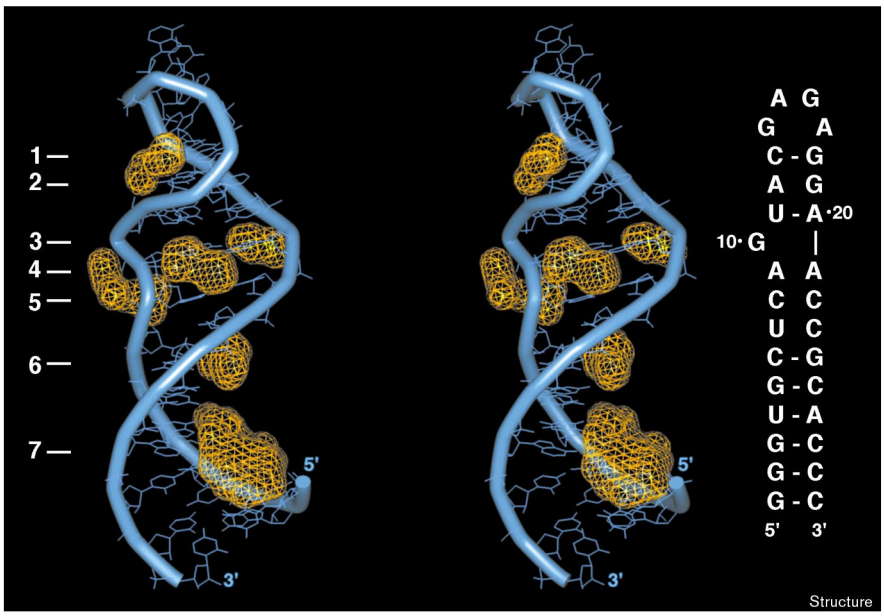

The NMR structure of a 35-nucleotide RNA aptamer that specifically binds FMN [56] is a particularly challenging case for the prediction of metal ion binding sites because the presence of Mg^{2+} is critical for the binding of the ligand to the aptamer [48]. It is not known whether divalent metal ions are required for correctly folding the RNA aptamer into a high-affinity conformation for the ligand FMN, or if Mg^{2+} is directly involved in mediating contacts between the RNA and the ligand. BD simulations on the aptamer RNA in the absence of the ligand FMN predict six possible sites for the binding of metal ions (Figure 8 and Table 1). Three of these sites (4–6) located at the lower stem extremity are probably not significant, as many contacts to nucleotides of the flexible 5′ and 3′ termini are

Figure 8

Stereoview of the NMR structure of an RNA aptamer for FMN [56]. Predicted binding sites (1–6) for metal ions are shown as density grids, as in Figure 2. On the right-hand side, the secondary structure of the aptamer, as inferred from the pairing and stacking pattern in the NMR structure, is depicted. The ligand FMN (magenta) binds to the internal bulge by intercalation between the $G_9 \cdot G_{27}$ mismatch pair and a base triple formed by $G_{10} \cdot U_{12} \cdot A_{25}$.

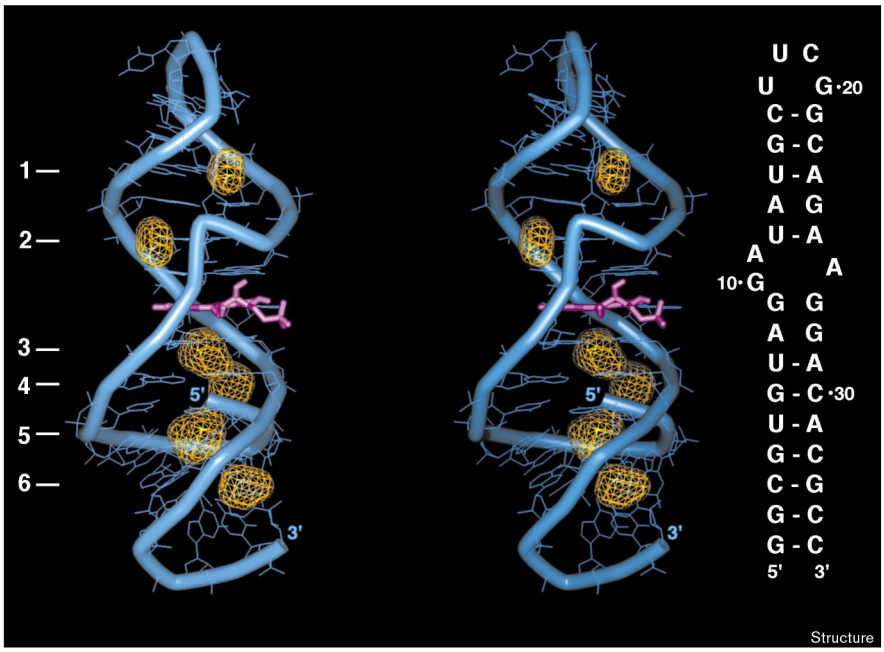

Figure 9

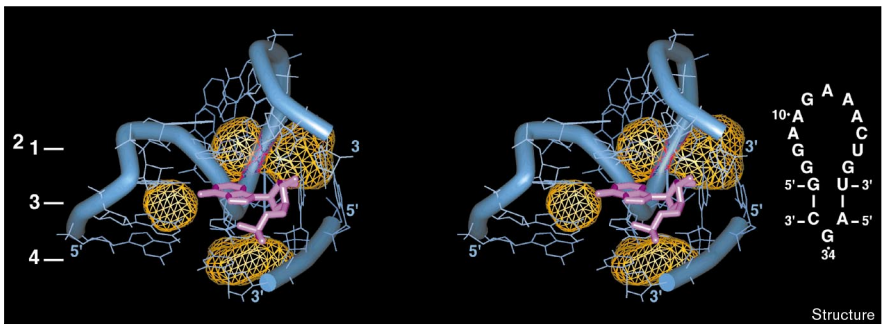

Stereoview of the three-dimensional solution structure of an RNA aptamer–AMP complex determined by NMR spectroscopy [57]. Only the core region comprising the binding site for the ligand AMP (magenta) is shown. Predicted binding sites (1–4) for metal ions are marked as density grids, as in Figure 2. A representation of the secondary structure is shown on the right.

involved. Differences in the prediction of negatively charged pockets were mainly observed in this region when two different conformers from the NMR data set, which deviated from each other in the terminal region, were used. The stem connecting the ligand pocket and the UNCG-type loop, where N is any nucleotide [54], harbours a putative metal ion binding site (1) that may be responsible for the stabilization of the nonconserved bulged A_{11} base in the deep groove. Two of the predicted metal sites (2 and 3) involve nucleotides of the ligand pocket, which comprises G_9, G_{10}, U_{12}, and A_{25}–G_{27} [56]. At sites 2 and 3, metal binding is likely to be both sequence and structure specific, indicated by the fact that nucleotide bases are essentially participating in the metal contacts: a metal ion at site 2 would interact with the base of G_{10}; site 3 is formed by the bases of G_9 and G_{27} along with the A_{26} phosphate. Although, for geometrical reasons, a direct contact between a metal ion bound at site 3 to the intercalated FMN ligand is unlikely, hydrogen bonding between a water molecule of the hydration shell of, for example, Mg^{2+} to either the carbonyl O4 or N5 of FMN is possible. Thus, it could be envisaged that the experimentally observed Mg^{2+} dependence of FMN binding to the RNA aptamer [48,56] is due to the stabilizing function of a Mg^{2+} bound at the predicted site 3.

The three-dimensional structure of an RNA aptamer for ATP complexed to AMP has been solved by NMR spectroscopy, revealing an S-shaped fold with a GNRA-loop-like structure at the intersection of two perpendicular helical stems [57]. Strikingly, the noncovalently bound ligand AMP provides the fourth base of the GNRA motif, although it participates in a different base-pairing scheme. An intricate assembly of stacked purines forms the core of the aptamer–AMP complex, giving rise to a number of pockets that are probably suitable for metal ion binding. In BD simulations on the RNA aptamer–AMP complex, we identified four independent metal ion binding sites (Figure 9 and Table 1). All four predicted sites are located in the hinge between the perpendicular helices and therefore involve nucleotides participating in ligand binding, but not of the AMP ligand itself. The suggested metal ion binding sites occupy pockets in the purine core, opposite the ligand-binding site where the sugar-phosphate backbone of the RNA is tightly folded. It is likely that positively charged metal ions are required for electrostatic neutralization of close phosphate charges, in order to allow the proper folding of the aptamer upon ligand binding.

Biological implications

RNA plays an important role in many key biological processes. The function of RNA is closely linked to its three-dimensional structure. It is now generally accepted that RNA can fold into structured domains with recurring interaction motifs. Metal ions constitute an integral part of RNA structure where they neutralize backbone phosphate charges, participate in folding, and provide catalytically reactive centers. The positions of metal ions are still only known for relatively few three-dimensional RNA structures derived by X-ray crystallography. Solution studies have shown that, in addition to the crystallographically identified sites, many more metal ion binding sites exist in RNA. In NMR analysis of RNA structures metal ions are usually present, but standard NMR techniques do not reveal their positions.

Here, we present a novel method for the prediction of metal ion binding sites in RNA folds. The prediction method is based on the analysis of simulated trajectories of positively charged probes diffusing under the influence of both random Brownian motion and the electrostatic field extending from the target RNA molecule. The method takes into account the shape and gradient of the electrostatic field, both of which are responsible for funneling cations towards negatively charged pockets of the RNA fold. This novel approach allows a semi-quantitative assessment of the binding sites and is therefore superior to methods based on the inspection of the electrostatic potential at a given surface of an RNA molecule.

The prediction method successfully reproduces the crystallographically determined positions of Mg^{2+} ions in several different RNA molecules. A number of additional cation-binding sites have been detected in tRNAs, which are known from solution experiments to bind a greater number of metal ions than the crystallographically identified Mg^{2+} ions. A conserved metal ion binding site was identified in three different RNA structures in the deep groove of the 5′-GU-3′/3′-YG-5′ motif. This example of a conserved structural motif involving the participation of metal ions extends the small repertoire of structural fragments recurrent in various RNA folds.

The most promising application of the prediction method is the exploration of metal ion binding sites in NMR structures of RNA, for which information on the position of metal ions is usually not available. It could be envisaged that, in future, prediction of metal ion binding sites might be routinely used following determination of the three-dimensional fold of an RNA molecule.

Materials and methods

RNA structures

Atom coordinates were extracted from the Brookhaven Protein Data Bank (PDB) for loop E of bacterial 5S rRNA (354D [12]), $tRNA^{Phe}$ (4TRA [25]), $tRNA^{Asp}$ (3TRA [26]), the hammerhead RNA (301D [38]), the domain P4–P6 (1GID [11]) and the P5b stem loop of a group I intron (1AJF [18]), an RNA pseudoknot (1RNK [46]), the sarcin/ricin loop of eucaryal 28S rRNA (1SCL [53]), the AMP aptamer (1AM0 [57]), and the FMN aptamer (1FMN [56]). For the NMR-derived structures 1SCL, 1AM0, and 1FMN, several coordinate sets are available in the PDB file. In the cases of 1SCL and 1AM0, for which the individual models are very similar, we chose the first coordinate set for each. For 1FMN, we used two individual conformers that deviated mainly in the terminal region, away from the interesting FMN binding site that is very similar in all available coordinate sets. For crystal structures, Mg^{2+} ions were removed, hydrogen atoms added and energy refined under the AMBER forcefield [58] in the presence of explicit solvent by using previously described protocols [43].

Electrostatics

Electrostatics was treated with the non-linear Poisson-Boltzmann equation using a continuum model for the solvent with a dielectric constant of $78\varepsilon_0$ for water and $4\varepsilon_0$ for RNA. Atomic partial charges for RNA were from the AMBER 4.1 forcefield [58]. The grid spacing for calculation of the electrostatic field was 1.25 Å, except for the tRNAs for which a larger spacing of 1.4 Å was chosen. Visualization of electrostatic surface charge and field lines (Figure 1a) was done with GRASP [59]. For the calculation of field lines, water molecules from the first shell of hydration of the RNA were used as seed points. One field line emerging per water oxygen atom was drawn.

BD simulations

BD simulations were performed on rigid RNA targets and diffusible metal ions with the UHBD program [20]. The diffusing metal ions were modelled as spherical probes of radii between 1.0 and 3.0 Å and +2e charge. Trajectories of the diffusing test spheres were initiated at randomly chosen points at a distance of $r = 100$ Å from the center of mass of the RNA molecule, except for tRNAs for which the starting distance was 200 Å (Figure 1). Trajectories exceeding an outer cutoff sphere of radius $q = 200$ Å (400 Å for tRNAs) were terminated. Test spheres that stayed within the cutoff sphere were uniformly simulated for 200 ns at a time step of 0.02 ps. Trajectory coordinates were recorded at intervals of 200 ps. For each probe radius, 1000 trajectories (2000 for tRNAs) were calculated. The number of calculated trajectories did not influence the subsequent determination of metal ion binding sites, however, as long as more than several hundred trajectories were used for statistical evaluation.

Determination of metal ion binding sites

For each set of BD trajectories, the probability of finding the center of the charged probe within a discrete volume element in space was calculated on a cubic 1 Å grid (Equation 1). From the trajectories that stayed inside the cutoff sphere, the final 100 recorded steps, corresponding to the last 20 ns of the simulation, were used for the evaluation.

$$R_{X,Y,Z} = \frac{1}{sN}\sum_{l=1}^{N}\sum_{m=n-s}^{n}\delta\left(x_{l,m},y_{l,m},z_{l,m}\right),$$

$$\text{with } \delta(x,y,z) = \begin{cases} 1 & \text{for: } x = X, y = Y, z = Z \\ 0 & \text{otherwise} \end{cases}$$

(N = number of trajectories, n = total steps of a trajectory, s = number of steps used for evaluation)

The probabilities were visualized as a density grid superimposed on the RNA structure. While the calculated $R_{X,Y,Z}$ in principle reflects the affinity of a given site for the binding of positively charged spheres, we did not attempt a strict quantitative ranking of single predicted binding sites since additional effects influencing binding strength, such as the presence of solvent molecules, were neglected in our model calculations. The core density used for visualization (Figures 2–7) and calculation of ion positions was typically chosen to comprise such volume elements where $R_{X,Y,Z} > 0.01$, i.e. where at least 1000 events of a captured probe were counted per 1000 trajectories of probes that had hit the RNA. By choosing appropriate cutoff values for $R_{X,Y,Z}$, an approximate ranking of predicted metal ion binding sites according to the occupation of volume elements, similar to the rating by occupation factors in X-ray data, was possible.

Acknowledgements

TH is supported by an EMBO long-term fellowship. EW thanks the Institut Universitaire de France for providing grants.

References

1. Teeter, M.M., Quigley, G.J. & Rich, A. (1980). Metal ions and transfer RNA. In *Nucleic acid–metal ion interactions.* (Spiro, T.G., ed.), pp. 145-177, Wiley, New York.
2. Pan, T., Long, D.M. & Uhlenbeck, O.C. (1993). Divalent metal ions in RNA folding and catalysis. In *The RNA world.* (Gesteland, R.F. & Atkins, J.F., eds), pp. 271-302, Cold Spring Harbor Laboratory Press, New York.
3. Pyle, A.M. (1993). Ribozymes: a distinct class of metalloenzymes. *Science* **261**, 709-714.
4. Cate, J.H. & Doudna, J.A. (1996). Metal-binding sites in the major groove of a large ribozyme domain. *Structure* **4**, 1221-1229.
5. Holbrook, S.R., Sussman, J.L., Warrant, R.W., Church, G.M. & Kim, S.H. (1977). RNA-ligand interactions. (I) Magnesium binding sites in yeast $tRNA^{Phe}$. *Nucleic Acids Res.* **4**, 2811-2820.
6. Jack, A., Ladner, J.E., Rhodes, D., Brown, R.S. & Klug, A. (1977). A crystallographic study of metal-binding to yeast phenylalanine transfer RNA. *J. Mol. Biol.* **111**, 315-328.
7. Quigley, G.J., Teeter, M.M. & Rich, A. (1978). Structural analysis of spermine and magnesium ion binding to yeast phenylalanine transfer RNA. *Proc. Natl Acad. Sci. USA* **75**, 64-68.
8. Westhof, E. & Sundaralingam, M. (1986). Restrained refinement of the monoclinic form of yeast phenylalanine transfer RNA. Temperature factors and dynamics, coordinated waters, and base-pair propeller twist angles. *Biochemistry* **25**, 4868-4878.
9. Pley, H.W., Flaherty, K.M. & McKay, D.B. (1994). Three-dimensional structure of a hammerhead ribozyme. *Nature* **372**, 68-74.
10. Scott, W.G., Finch, J.T. & Klug, A. (1995). The crystal structure of an all-RNA hammerhead ribozyme: a proposed mechanism for RNA catalytic cleavage. *Cell* **81**, 991-1002.
11. Cate, J.H., *et al.*, & Doudna, J.A. (1996). Crystal structure of a group I ribozyme domain: principles of RNA packing. *Science* **273**, 1678-1685.

12. Correll, C.C., Freeborn, B., Moore, P.B. & Steitz, T.A. (1997). Metals, motifs, and recognition in the crystal structure of a 5S rRNA domain. *Cell* **91**, 705-712.
13. Schreier, A.A. & Schimmel, P.R. (1974). Interaction of manganese with fragments, complementary fragment recombinations, and whole molecules of yeast phenylalanine specific transfer RNA. *J. Mol. Biol.* **86**, 601-620.
14. Stein, A. & Crothers, D.M. (1976). Equilibrium binding of magnesium(II) by Escherichia coli $tRNA^{fMet}$. *Biochemistry* **15**, 157-160.
15. Gueron, M. & Leroy, J.L. (1982). Significance and mechanism of divalent-ion binding to transfer RNA. *Biophys. J.* **38**, 231-236.
16. Shen, L.X., Cai, Z. & Tinoco, I. Jr. (1995). RNA structure at high resolution. *FASEB J.* **9**, 1023-1033.
17. Ramos, A., Gubser, C.C. & Varani, G. (1997). Recent solution structures of RNA and its complexes with drugs, peptides and proteins. *Curr. Opin. Struct. Biol.* **7**, 317-323.
18. Kieft, J.S. & Tinoco, I. Jr. (1997). Solution structure of a metal-binding site in the major groove of RNA complexed with cobalt(III) hexammine. *Structure* **5**, 713-721.
19. Gdaniec, Z., Sierzputowska-Gracz, H. & Theil, E.C. (1998). Iron regulatory element and internal loop/bulge structure for ferritin mRNA studied by cobalt(III) hexammine binding, molecular modeling, and NMR spectroscopy. *Biochemistry* **37**, 1505-1512.
20. Madura, J.D., Davis, M.E., Gilson, M.K., Wade, R.C., Luty, B.A. & McCammon, J.A. (1994). Biological applications of electrostatic calculations and Brownian dynamics simulations. *Rev. Comput. Chem.* **5**, 229-267.
21. Honig, B. & Nicholls, A. (1995). Classical electrostatics in biology and chemistry. *Science* **268**, 1144-1149.
22. Leontis, N.B. & Moore, P.B. (1984). A small angle X-ray study of a fragment derived from E. coli 5S RNA. *Nucleic Acids Res.* **12**, 2193-2203.
23. Gessner, R.V., Quigley, G.J., Wang, A.-H.J., van der Marel, G.A., van Bloom, J.H. & Rich, A. (1985). Structural basis for stabilization of Z-DNA by cobalt hexammine and magnesium cations. *Biochemistry* **24**, 237-240.
24. Kim, S.-H., Quigley, G.J., Suddath, F.L., McPherson, A., Sneden, D., Kim, J.J., Weinzierl, J. & Rich, A. (1973). Three-dimensional structure of yeast phenylalanine transfer RNA: Folding of the polynucleotide chain. *Science* **179**, 285-288.
25. Westhof, E., Dumas, P. & Moras, D. (1988). Restrained refinement of two crystalline forms of yeast aspartic acid and phenylalanine transfer RNA crystals. *Acta Cryst. A* **44**, 112-123.
26. Westhof, E., Dumas, P. & Moras, D. (1985). Crystallographic refinement of yeast aspartic acid transfer RNA. *J. Mol. Biol.* **184**, 119-145.
27. Brown, R.S., Dewan, J.C. & Klug, A. (1985). Crystallographic and biochemical investigations of the lead(II)-catalyzed hydrolysis of yeast phenylalanine tRNA. *Biochemistry* **24**, 4785-4801.
28. Auffinger, P. & Westhof, E. (1997). RNA hydration: three nanoseconds of multiple molecular dynamics simulations of the solvated $tRNA^{Asp}$ anticodon hairpin. *J. Mol. Biol.* **269**, 326-341.
29. Saenger, W. (1984). *Principles of Nucleic Acid Structure*. Springer-Verlag, New York.
30. Masquida, B. & Westhof, E. (1997). Crystallographic structures of RNA oligoribonucleotides and ribozymes. In *Oxford Handbook of Nucleic Acid Structure*. (Neidle, S., ed.), London, in press.
31. Rubin, J.R., Wang, J. & Sundaralingam, M. (1983). X-ray diffraction study of the zinc(II) binding sites in yeast $tRNA^{Phe}$. *Biochem. Biophys. Acta* **756**, 111-118.
32. Birikh, K.R., Heaton, P.A. & Eckstein, F. (1997). The structure, function and application of the hammerhead ribozyme. *Eur. J. Biochem.* **245**, 1-16.
33. Bassi, G.S., Murchie, A.I.H. & Lilley, D.M.J. (1996). The ion-induced folding of the hammerhead ribozyme: Core sequence changes that perturb folding into the active conformation. *RNA* **2**, 756-768.
34. Bassi, G.S., Murchie, A.I.H., Walter, F., Clegg, R.M. & Lilley D.M.J. (1997). Ion-induced folding of the hammerhead ribozyme - a fluorescence resonance energy transfer study. *EMBO J.* **16**, 7481-7489.
35. Dahm, S.C. & Uhlenbeck, O.C. (1991). Role of divalent metal ions in the hammerhead RNA cleavage reaction. *Biochemistry* **30**, 9464-9469.
36. Dahm, S.C., Derrick, W.B. & Uhlenbeck, O.C. (1993). Evidence for the role of solvated metal hydroxide in the hammerhead cleavage reaction. *Biochemistry* **32**, 13040-13045.
37. Hermann, T., Auffinger, P., Scott, W.G. & Westhof, E. (1997). Evidence for a hydroxide ion bridging two magnesium ions at the active site of the hammerhead ribozyme. *Nucleic Acids Res.* **25**, 3421-3427.
38. Scott, W.G., Murray, J.B., Arnold, J.R.P., Stoddard, B.L. & Klug, A. (1996). Capturing the structure of a catalytic RNA intermediate: the hammerhead ribozyme. *Science* **274**, 2065-2069.
39. Chartrand, P., Leclerc, F. & Cedergren, R. (1997). Relating conformation, Mg^{2+} binding, and functional group modification in the hammerhead ribozyme. *RNA* **3**, 692-696.
40. Feig, A.L., Scott, W.G. & Uhlenbeck, O.C. (1998). Inhibition of the hammerhead ribozyme cleavage reaction by site-specific binding of Tb(III). *Science* **279**, 81-84.
41. Menger, M., Tuschl, T., Eckstein, F. & Pörschke, D. (1996). Mg^{2+}-Dependent conformational changes in the hammerhead ribozyme. *Biochemistry* **35**, 14710-14716.
42. Long, D.M., LaRiviere, F.J. & Uhlenbeck, O.C. (1995). Divalent metal ions and the internal equilibrium of the hammerhead ribozyme. *Biochemistry* **34**, 14435-14440.
43. Hermann, T., Auffinger, P., & Westhof, E. (1998). Molecular dynamics investigations of hammerhead ribozyme RNA. *Eur. Biophys. J.* **27**, 153-165.
44. Murray, J.B., *et al.*, & Scott, W.G. (1998). The structural basis of hammerhead ribozyme self-cleavage. *Cell* **92**, 665-673.
45. Hermann, T. & Westhof E. (1998). Aminoglycoside binding to the hammerhead ribozyme: a general model for the interaction of cationic antibiotics with RNA. *J. Mol. Biol.* **276**, 903-912.
46. Shen, L.X. & Tinoco, I. Jr. (1995). The structure of an RNA pseudoknot that causes efficient frameshifting in mouse mammary tumor virus. *J. Mol. Biol.* 247, 963-978.
47. Glück, A., Endo, Y. & Wool, I.G. (1992). Ribosomal RNA identity elements for ricin A-chain recognition and catalysis. *J. Mol. Biol.* **226**, 411-424.
48. Burgstaller, A.T. & Famulok, M. (1994). Isolation of RNA aptamers for biological cofactors by in vitro selection. *Angew. Chem. Int. Ed. Eng.* **33**, 1084-1087.
49. Sassanfar, M. & Szostak, J.W. (1993). An RNA motif that binds ATP. *Nature* **364**, 550-553.
50. Patel, D.J., *et al.*, & Nonin, S. (1997). Structure, recognition and adaptive binding in RNA aptamer complexes. *J. Mol. Biol.* **272**, 645-664.
51. Wyatt, J.R & Tinoco, I. Jr. (1993). RNA structural elements and RNA function. In *The RNA World*. (Gesteland, R.F. & Atkins, J.F., eds), pp. 465-496, Cold Spring Harbor Laboratory Press, New York.
52. Wyatt, J.R, Puglisi, J.D. & Tinoco, I. Jr. (1990). RNA pseudoknots: stability and loop size requirements. *J. Mol. Biol.* **214**, 455-470.
53. Szewczak, A.A. & Moore, P.B. (1995). The sarcin/ricin loop, a modular RNA. *J. Mol. Biol.* **247**, 81-98.
54. Woese, C.R., Winker, S. & Gutell, R.R. (1990). Architecture of ribosomal RNA - Constraints on the sequence of tetra-loops. *Proc. Natl Acad. Sci. USA* **87**, 8467-8471.
55. Monzingo, A.F. & Robertus, J.D. (1992). X-ray analysis of substrate analogs in the ricin A chain active site. *J. Mol. Biol.* **227**, 1136-1145.
56. Fan, P., Suri, A.K., Fiala, R., Live, D. & Patel, D.J. (1996). Molecular recognition in the FMN-RNA aptamer complex. *J. Mol. Biol.* **258**, 480-500.
57. Jiang, F., Kumar, R.A., Jones, R.A. & Patel, D.J. (1996). Structural basis of RNA folding and recognition in an AMP-RNA aptamer complex. *Nature* **382**, 183-186.
58. Cornell, W.D., *et al.*, & Kollman, P.A. (1995). A second generation force field for the simulation of proteins, nucleic acids and organic molecules. *J. Am. Chem. Soc.* **117**, 5179-5197.
59. Nicholls, A., Sharp, K.A. & Honig, B. (1991) Protein folding and association: insights from the interfacial and thermodynamic properties of hydrocarbons. *Proteins* **11**, 281-96.